

Robotic Arm for Remote Surgery

Steven Dinger*, John Dickens and Adam Pantanowitz†

Abstract

Recent advances in telecommunications have enabled surgeons to operate remotely on patients with the use of robotics. The investigation and testing of remote surgery using a robotic arm is presented. The robotic arm is designed to have four degrees of freedom that track the surgeon's x , y , z positions and the rotation angle of the forearm θ . The system comprises two main subsystems *viz.* the detecting and actuating systems. The detection system uses infrared light-emitting diodes, a retroreflective bracelet and two infrared cameras which as a whole determine the coordinates of the surgeon's forearm. The actuation system, or robotic arm, is based on a lead screw mechanism which can obtain a maximum speed of 0.28 m.s^{-1} with a $1.5^\circ \text{.step}^{-1}$ for the end-effector. The infrared detection and encoder resolutions are below $0.6 \text{ mm.pixel}^{-1}$ and 0.4 mm respectively, which ensures the robotic arm can operate precisely. The surgeon is able to monitor the patient with the use of a graphical user interface on the display computer. The lead screw system is modelled and compared to experimentation results. The system is controlled using a simple proportional-integrator (PI) control scheme which is implemented on a dSpace control unit. The control design results in a rise time of less than 0.5 s , a steady-state error of less than 1 mm and settling time of less than 1.4 s . The system accumulates, over an extended period of time, an error of approximately 4 mm due to inertial effects of the robotic arm. The results show promising system performance characteristics for a relatively inexpensive solution to a relatively advanced application.

Keywords: Remote surgery, PI controller, lead screw, optical encoder, infrared light emitting diode.

*S. Dinger is with the Biomedical Engineering Research Group, School of Electrical & Information Engineering, University of Witwatersrand, Johannesburg, e-mail: steven.dinger@wits.ac.za.

†J. Dickens and A. Pantanowitz are with the Biomedical Engineering Research Group, School of Electrical & Information Engineering, University of Witwatersrand, Johannesburg.

1 Background

Remote surgery or telesurgery enables a surgeon to operate on a patient who is at a different geographical location. The use of robotics in surgery has improved the accuracy and capabilities of surgeon's significantly in recent years [1]. The major drawback, however, with current systems is that the surgeon is usually required to control the robotic device in an uncomfortable position with the device usually vulnerable to human tremors and operator fatigue [2].

The concept of remote surgery is explored and tested with the use of a robotic arm that is able to mimic the movement of a surgeon's forearm. The robotic arm is designed to have four degrees of freedom *viz.* the x , y , z positions and rotation angle θ of the forearm. The simplest requirement of the robotic arm is to track the movements of a surgeon's forearm precisely and to operate in an identical workspace to that of a typical surgeon.

The three types of human movement detection systems are the inside-in, outside-in and inside-out detection systems [3]. The use of an accelerometer to detect three-dimensional movement is a feasible technology and represents an inside-in type system [4]. The use of potentiometers, piezo-resistive flex and cable extension represent examples of outside-in type systems [3], however they suffer from drift.

A spherical design of the robotic arm overcomes many of the problems faced in robotics, such as reducing the size and weight of the robotic instrument [5]. The reachable workspace, however, for a spherical robotic arm is limited to a sector of a sphere, and is therefore not desirable in terms of reproducing the complete operating workspace of the surgeon.

The telesurgery robotic arm comprises two major non-located subsystems, *viz.* the detection and actuation system. The coordination between the two systems can be achieved through the use of current telecommunications technology [1].

This paper specifies the system requirements, constraints and assumptions that are used to effectively implement such a system. The layout of the system is presented and covers the two main subsystems, *viz.* the detection system and the actuation system. The lead screw system is modelled and used to compare to the experimentation results. The controller used for the robotic arm is also discussed. The simulation and experimentation results are provided and analysed in order to determine the performance of the system. The system limitations are listed including recommendations and suggestions for future work. A conclusive summary pertaining to the performance and fundamental aspects of the system is given.

2 System Specifications

The forearm of a surgeon is considered to have four degrees of freedom, which include the x , y , z positions and rotation of the forearm denoted as θ . A satisfactory design, therefore, includes the ability of the robotic arm to mimic and track the surgeon's forearm for all four degrees of freedom.

The delay of the control signal of the system must be less than 500 ms for the surgeon to successfully compensate for the latency during the operating procedure [6]. Visual feedback is required in order for the surgeon to monitor the patient and correct for any error that accumulates during the procedure. The tracking error is considered more important as opposed to the steady-state error, since the steady-state error can be easily corrected by the surgeon through the visual feedback system. The system must be able to be calibrated to remove any cumulative error that occurs during operation.

A constraint on the amount of wrist pitch and forearm flexion of the surgeon exists mainly due to the outside-in type of detection system employed [3]. The outside-in detection system uses artificial sources placed on the body with the sensors situated externally.

2.1 Assumptions

The assumptions used to design, implement and operate the system successfully are:

- Pitch of the surgeon's hand is negligible during an operation.
- A maximum speed of $0.25 \text{ m}\cdot\text{s}^{-1}$ for each axis is deemed satisfactory.
- The workspace of the surgeon is devoid of infrared noise.

The assumption that the hand pitch is negligible is necessary, since the detection sources are placed on the hand as described in Section 3.1. A maximum speed of $0.25 \text{ m}\cdot\text{s}^{-1}$ is reasonable, since a surgeon's forearm should remain in the same anatomical region throughout the operation, with the hand performing most of the fast and precise movements. A speed of $0.25 \text{ m}\cdot\text{s}^{-1}$, which was measured experimentally, is also relatively large for a typical human forearm to move. The workspace should be illuminated with fluorescent lighting in order to reduce infrared noise.

3 System Architecture

The system comprises two main subsystems *viz.* the detection and actuation systems. The block diagram that illustrates how the two systems are coordinated and linked as shown in Figure 1.

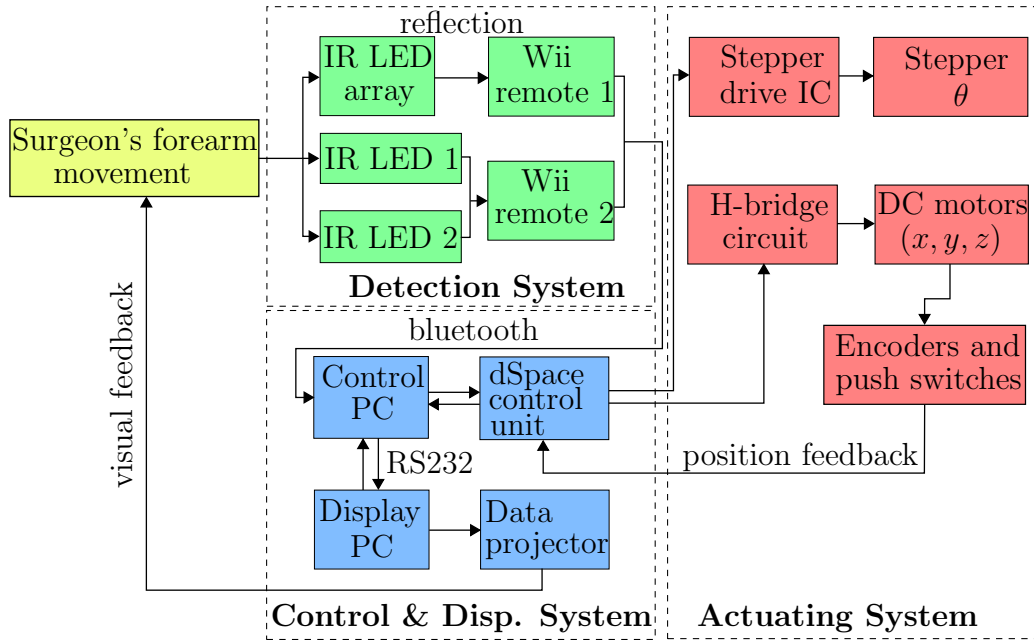


Figure 1: System block diagram.

3.1 Detection System

The movement of the surgeon's forearm is detected using a non-invasive outside-in detection system, which consists of placing the sensors off, and artificial sources on, the person. The artificial sources used are two infrared (940 nm) light emitting diodes (LEDs) and a retroreflective bracelet.

The two infrared LEDs are located in the region of the proximal phalanges and are used to measure the z -axis position of the surgeon's arm, including the forearm rotation angle θ , as shown in Figure 2. Two Nintendo Wii remotes are used to capture and process the data obtained from the infrared sources and reflections. The Wii remote infrared (940 nm) camera has a resolution of 1024×768 , which at the heights and distances shown in Figure 2, provides a resolution of $0.586 \text{ mm.pixel}^{-1}$ for x and z axes, and $0.576 \text{ mm.pixel}^{-1}$ for the y axis. A retroreflective wrist band is used as opposed to infrared LEDs in order for the Wii remote to continue tracking the

forearm under rotation. A 132-LED array is used to produce the infrared light source for the reflective wrist band [7].

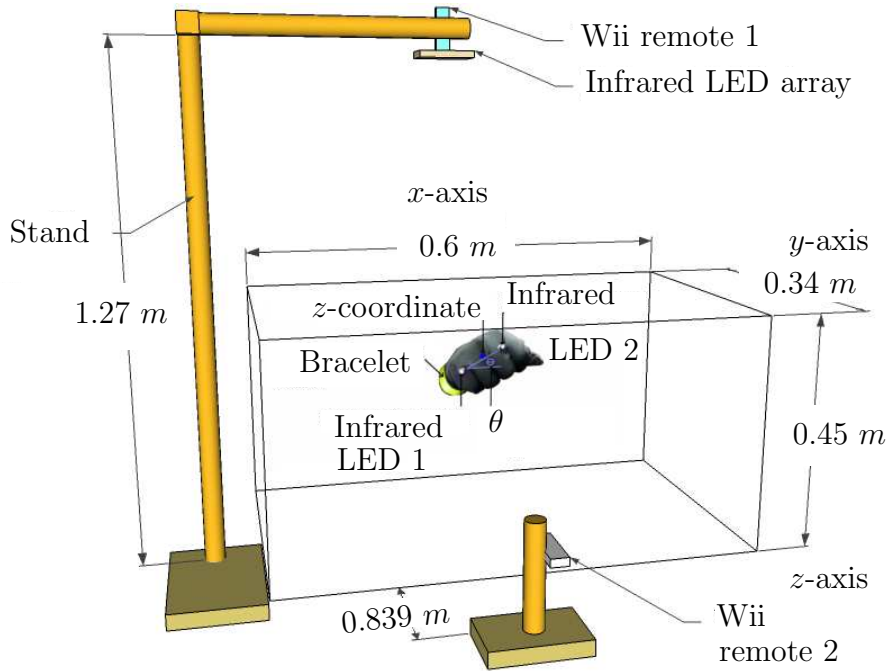


Figure 2: Illustration of the infrared detection system.

3.2 Actuation system

The actuation system is illustrated in Figure 3, and includes the optical encoders that measure the position of the carrier blocks and calibration switches located on each axis. The robotic arm follows a simple lead-screw guide-rail design, with the advantages of the design being:

- No energy consumption at rest.
- Stable and rigid.
- Lightweight and modular.
- Simple to construct and control.

The disadvantages of the design include a low mechanical efficiency due to excessive amounts of dynamic friction [8]. The non-linear static friction in the system causes a deadzone effect, whereby the control signal has no effect

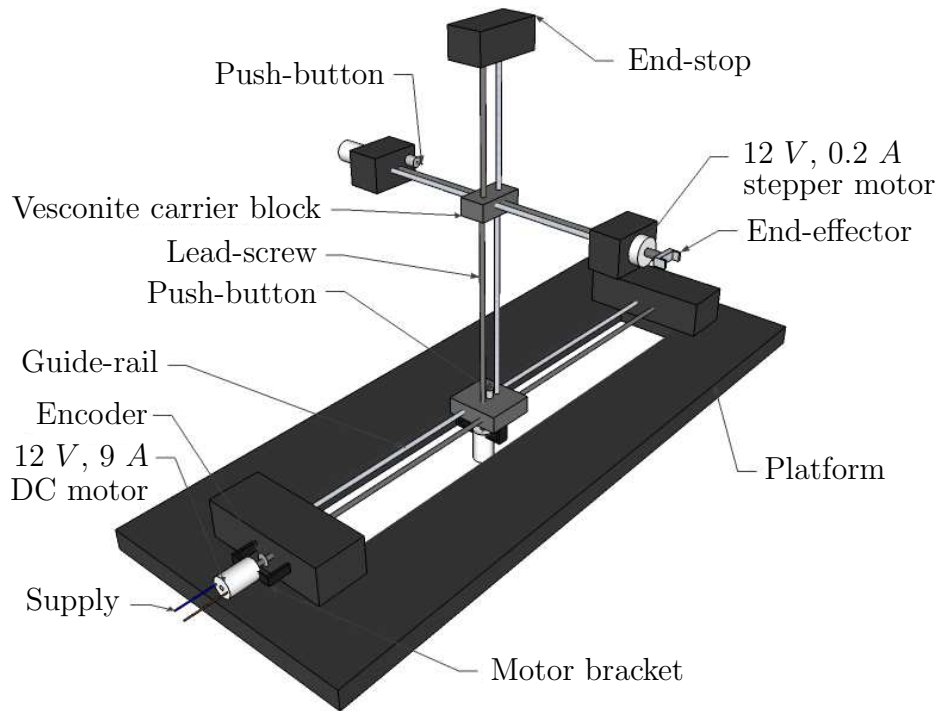


Figure 3: Illustration of the mechanical robotic arm.

on the system within a certain armature voltage range. The fine standard pitch used for the lead screws is 1.5 mm for the x and z axes, and 1.25 mm for the y axis. The size of pitch requires large angular speeds (17000 rpm) to generate modest linear speeds. The large angular speeds cause mechanical vibrations, an increase in friction (heat losses) and significant audible noise.

4 Control

4.1 System Interfacing

The detected infrared information is processed and conditioned as inputs for the *dSpace* 1104 control unit. The desired coordinates are written to *dSpace* using the commands and functions supplied by the Matlab library called *mlib*.

The *dSpace* unit interfaces with the actuation system and communicates with the control computer. The model of the controller is built in the Matlab Simulink environment, including the necessary routing such as the inputs from the encoders and outputs to the logic and pulse-width modula-

tion (PWM) channels.

The $1.5 \text{ }^\circ.\textit{step}^{-1}$ geared stepper motor has no feedback and is rotated using open-loop, single-phase excitation [9][10]. A step frequency of 125 Hz is used, which results in an angular speed of 31.25 rpm .

4.2 System Modeling

The model of the system is presented and is used to obtain the gain values for the chosen proportional-integral (PI) controller. The assumptions used to model the system are listed below:

- Inelastic steel lead screw.
- Motor inductance is negligible.
- Static friction coefficient for lubricated metals.
- The lead screw moment of inertia is larger than that of the motor shaft.
- Mechanical power loss in the motor is negligible.

The assumption that elastic torsion of the threaded steel rod does not occur is validated since the rods are short in the lengths (less than 1 m). The mass accelerated by the motors is much larger than the inertia introduced by the inductance of the motor. The mass of the lead screw is much larger than that of the motor shaft, as shown in equation 6, which validates the assumption that the lead screw moment of inertia is greater than that of the motor shaft. The mechanical windage and frictional losses in the motor are assumed to be negligible in order to approximate the back-EMF constant K_b to the armature torque constant K_a , and is shown in detail by Sen [9].

The dynamics of the vertical (z -axis) lead screw are obtained with the gravitational acceleration ($g = 9.8 \text{ m/s}^2$) treated as a constant disturbance on the system. The system model diagram, consisting of the DC motor and lead screw, is shown in Figure 4. The system model diagram is used to derive the system equations by using Newton's laws of motion, with the relationship between motor torque and load weight provided by Hollander and Sugar [8]. The static friction coefficient is assumed to have a value of 0.06, which is the value for lubricated metals [8].

The definitions of the parameters and quantities used to describe the lead screw and motor system are given as:

- m - Load mass (kg)
- D - Dynamic friction coefficient ($N.s/m$)
- μ - Static friction coefficient
- r - Lead screw radius (m)
- L - Lead screw length (m)
- l - Pitch (m) (m/rev)
- K - Pitch constant (m/rad)
- τ_{motor} - Motor torque ($N.m$)
- $\tau_{inertia}$ - Lead screw inertial torque ($N.m$)
- τ_{mech} - Resultant mechanical torque ($N.m$)
- ω_m - Motor angular velocity (rad/s)
- R_a - Armature resistance (Ω)
- J_l - Lead screw moment of inertia ($kg.m^2$)

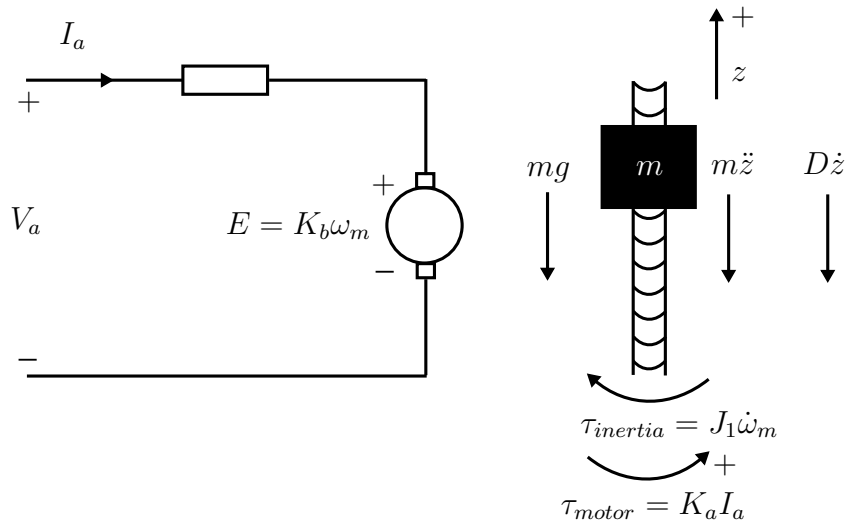


Figure 4: System model diagram.

The equation that describes the dynamics of the motor is obtained by using Kirchoff's voltage law, as shown in equation 1.

$$\begin{aligned}
V_a &= I_a R_a + K_b \omega_m & (1) \\
\tau_{mech} &= r F_w \frac{\sin\alpha + \mu \cos\alpha}{\cos\alpha - \mu \sin\alpha} \\
\alpha &= \arctan\left(\frac{l}{2\pi r}\right) \\
l &= 1.25 \text{ mm} \\
r &= 4 \text{ mm} \\
\therefore \alpha &= 2.847^\circ \\
\Rightarrow \tau_{mech} &= 0.4403 \times 10^{-3} \times F_w & (2)
\end{aligned}$$

Let:

$$\gamma = 0.4403 \times 10^{-3} \quad (3)$$

Define:

$$\tau_{mech} = \tau_{motor} - \tau_{inertia}$$

The resultant force F_w is the sum of the opposing forces acting on the mass for motion in the positive z -direction. The equation that describes the relationship between the torques and opposing forces is shown in equation 5.

$$F_w = D\dot{z} + mg + m\ddot{z} \quad (4)$$

$$\tau_{motor} - \tau_{inertia} = \gamma(D\dot{z} + mg + m\ddot{z}) \quad (5)$$

$$\dot{z} = K\omega_m$$

The mass accelerated by the vertical lead screw, m , is approximately 1.3 kg. The armature resistance of the brushed DC motor is provided by the data sheet with a value of 0.205 Ω [11]. The armature torque constant K_a is approximately $10.25 \times 10^{-3} \text{ N.m/A}$ [11]. The back-EMF constant K_b is the same as the armature constant with a value of $10.25 \times 10^{-3} \text{ V.s/rad}$. The pitch per radian of rotation K for the standard 8 mm diameter lead screw is calculated as $\frac{1.25 \times 10^{-3}}{2\pi}$, which is equal to $0.1989 \times 10^{-3} \text{ m/rad}$.

$$\begin{aligned}
\tau_{inertia} &= J_l \frac{d\omega_m}{dt} \\
\tau_{inertia} &= \frac{J_l}{K} \ddot{z} \\
J_l &= \frac{1}{2} M r^2 \\
M &= \pi r^2 L \rho_{steel} \\
\rho_{steel} &= 7850 \text{ kg/m}^3 \\
L &= 0.54 \text{ m} \\
\therefore M &= 0.213 \text{ kg} \\
\Rightarrow J_l &= 1.71 \times 10^{-6} \text{ kg.m}^2 \\
\therefore \frac{J_l}{K} &= 8.57 \times 10^{-3} \text{ kg.m.rad}
\end{aligned} \tag{6}$$

The two separate systems, motor and lead screw, are combined into one system with the appropriate substitutions shown in equation 7.

$$\begin{aligned}
V_a &= \frac{\tau_{motor}}{K_a} R_a + K_b \frac{\dot{z}}{K} \\
V_a &= \frac{R_a \gamma}{K_a} (D \dot{z} + mg + m \ddot{z}) + K_b \frac{\dot{z}}{K} + \frac{R_a}{K_a} \tau_{inertia} \\
\therefore V_a &= \left(\frac{R_a J_l}{K_a K} + \frac{R_a m \gamma}{K_a} \right) \ddot{z} + \left(\frac{D R_a \gamma}{K_a} + \frac{K_b}{K} \right) \dot{z} + \frac{R_a \gamma m g}{K_a}
\end{aligned} \tag{7}$$

$$\tag{8}$$

The dynamic friction coefficient D is determined from the experimentation results by estimating the constant maximum velocity (0.262 m/s), which occurs at maximum voltage of 13.8 V , and substituting the two values into equation 5 and equation 7. The dynamic friction value is calculated to be approximately 81 N.s/m , 80 N.s/m and 575.6 N.s/m for the z , x and y -axis lead screws respectively. The dynamic friction coefficient for the y -axis lead screw is significantly larger than the other two lead screws since it is driven by a different motor that has a fan attached to the motor shaft [12]. The simplified state-space representation of the system is obtained by substituting the listed variables and constants into equation 8.

$$\begin{aligned}
z &= x_1 & , V_a &= u_1 \\
\dot{z} &= x_2 = \dot{x}_1 & , g &= u_2 \\
\ddot{z} &= \dot{x}_2 = \ddot{x}_1 & , y_1 &= x_1 \\
K_1 &= \left(\frac{DR_a\gamma}{K_a} + \frac{K_b}{K} \right) & , y_2 &= x_2 \\
K_2 &= \left(\frac{R_a J_l}{K_a K} + \frac{R_a m \gamma}{K_a} \right) & , K_3 &= \frac{R_a \gamma m}{K_a}
\end{aligned}$$

The state equations are given as:

$$\begin{aligned}
\begin{bmatrix} \dot{x}_1 \\ \dot{x}_2 \end{bmatrix} &= \begin{bmatrix} 0 & 1 \\ 0 & \frac{-K_1}{K_2} \end{bmatrix} \begin{bmatrix} x_1 \\ x_2 \end{bmatrix} + \begin{bmatrix} 0 & 0 \\ \frac{1}{K_2} & \frac{-K_3}{K_2} \end{bmatrix} \begin{bmatrix} u_1 \\ u_2 \end{bmatrix} \\
\begin{bmatrix} y_1 \\ y_2 \end{bmatrix} &= \begin{bmatrix} 1 & 1 \end{bmatrix} \begin{bmatrix} x_1 \\ x_2 \end{bmatrix}
\end{aligned}$$

The non-linear friction in the system causes a deadzone effect to occur whereby the input control voltage is not able to move the mass until it is greater than a certain value. The value of the input voltage at which movement occurs was found through experimentation to be approximately $5 V$, $3 V$ and $3.4 V$ for the z , x and y -axis lead screws respectively. The deadzone effect is included in the Simulink s-function, which is used to model the system. The derived state equations hold for the other two axes by equating the gravitational acceleration input to zero and substituting in the appropriate masses, motor constants and other adjusted parameters.

4.3 Controller design

A classic controller is used for the robotic arm and comprises a proportional gain and integrator, with gain constants of $K_i = 150 V.m^{-1}.s^{-1}$ and $K_p = 55 V.m^{-1}$. The gain constants were determined from the model and refined through experimentation. The integrator is limited in order to prevent integrator-wind up [13]. All of the axes are controlled with identical controllers.

A derivative term was not used since it was found from experimentation that it amplified noise and increased the motor armature current significantly ($\Delta I_a = 3 A$). The controller was designed to optimize the actuation system in terms of power consumption, tracking error and rise time. The reduction of power consumption is achieved by switching the PWM off when the position error is within a $1 mm$ error band for a duration of $5 s$. The trade-off, however, is that there exists some steady-state and overshoot error in the step response.

5 System Performance and Analysis

The system performance was measured using sinusoid, ramp and step inputs. The rise time and tracking error are obtained from the step response and ramp response respectively. The steady-state error and settling time are also obtained from the step response of the system. The deadzone time is the duration that the system remains stationary due to non-linear friction, and is most evident in the sinusoidal response. The reliability of the system was measured by observing the accumulated error for a specified time limit. These results were compared to simulations based on the Newtonian models. The various system responses for the z -axis lead screw are shown in Figures 5, 6 and 7. The results for the other two axes are similar.

The overall results of the system performance in terms of responsiveness and resolutions are shown in Table 1. The encoder resolution is determined by dividing the lead screw pitch by the number of opaque sectors (4 dark segments per axis encoder).

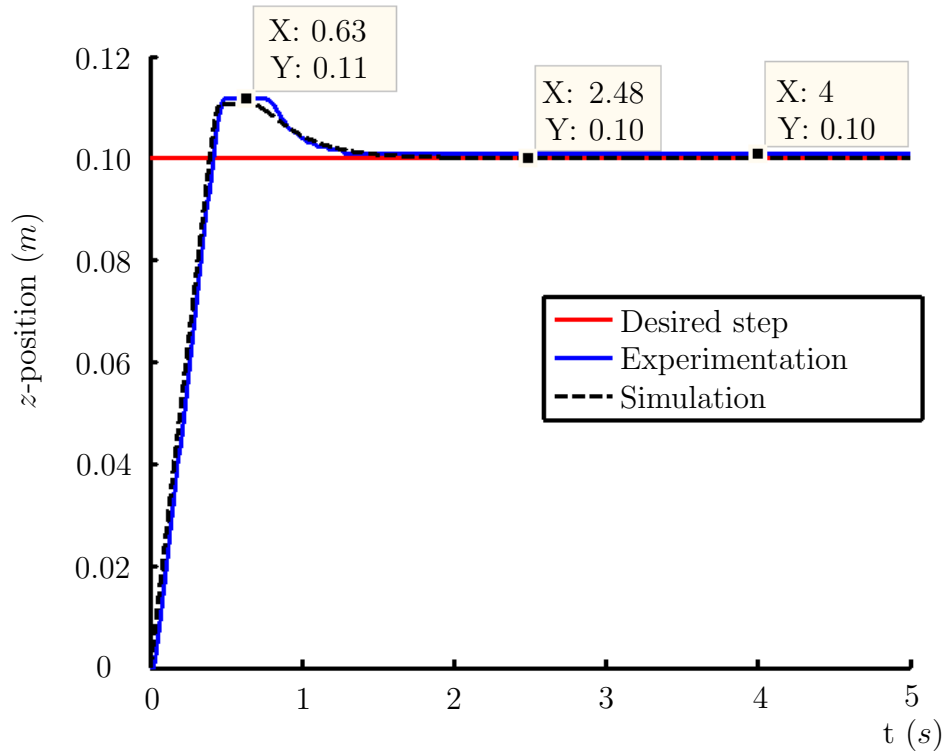


Figure 5: Step response of the z -axis lead screw.

Table 1: Experimentation results of system performance.

Parameter	x -axis	y -axis	z -axis
Steady-State Error (mm)	0.9	0.313	0.9
Rise Time (s)	0.35	0.28	0.41
Overshoot (%)	16	16.3	11.9
2 % Settling Time (s)	1.31	0.95	1.21
Deadzone Time (s)	0.33	0.35	0.33
Encoder Resolution (mm)	0.375	0.313	0.313
Resolution ($mm.pixel^{-1}$)	0.586	0.586	0.576

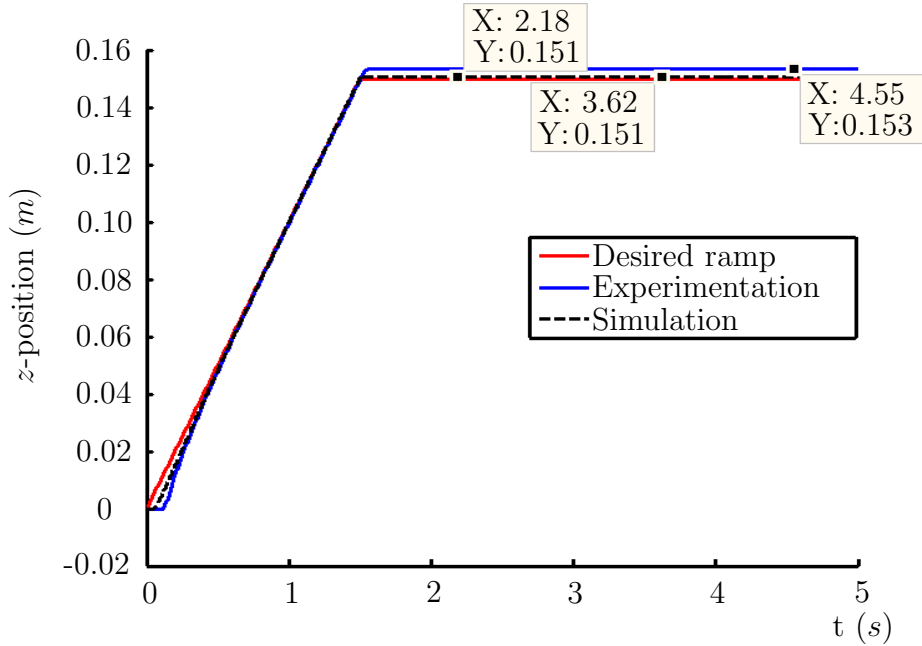


Figure 6: Ramp response of the z -axis lead screw.

The results show that the system is able to perform satisfactorily according to the success criteria stated in Section 2. It is noted that the rise time of y -axis lead screw is the fastest, which is due to the fact that the motor has a higher rated speed compared to the other two DC motors [12][11].

The error accumulation in the system was found to be a function of speed and sudden changes in motor direction. The cumulative error was therefore quantified using two different waveforms: a low-frequency sinusoid and a higher harmonic triangular waveform. The sinusoid and triangular waveforms were each applied separately for a duration 68 s and 41 s respectively. The offset error was recorded at the end of each test with the average results shown in Table 2.

The cumulative error is due to the inertia of the masses opposing sudden changes in velocity, and since the motor direction switches electronically, results in an increment or decrement of the position. The error therefore accumulates when there are sudden changes in direction at a reasonable speed. An error is also associated with the incremental measurement made by the low-cost optical encoders, which can be corrected by using alternative encoders. The error accumulation is largest as expected for the triangular waveform, as shown in Table 2.

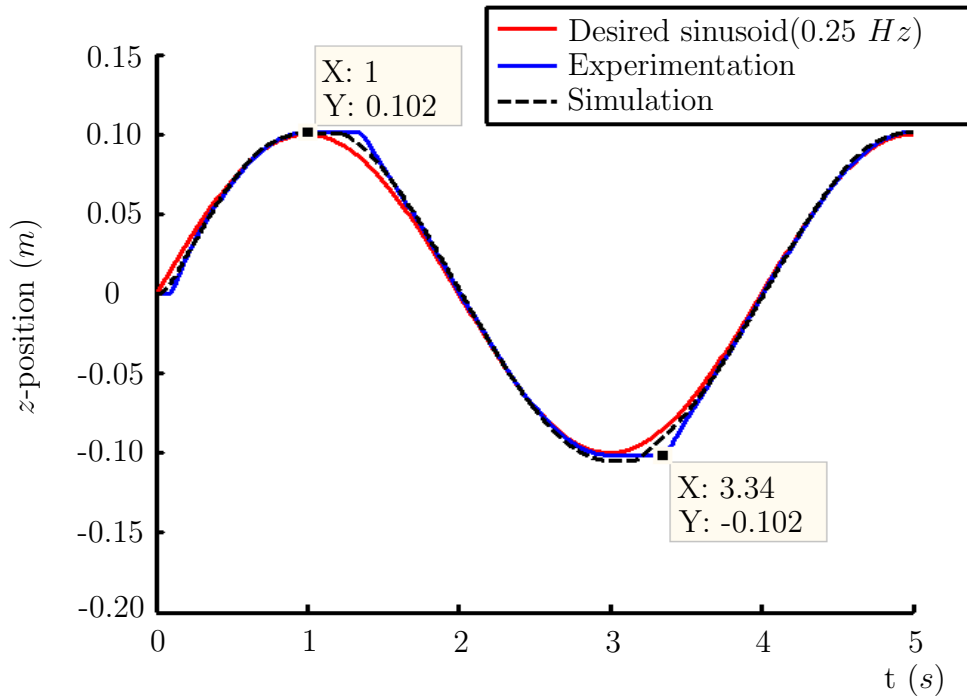


Figure 7: Sinusoidal response of the z -axis lead screw.

5.1 System limitations

The telesurgery robotic arm system has a number of limitations *viz.*:

- Average maximum speed of 0.28 m/s .
- Reasonable mechanical vibrations and resonance.
- Mechanical stability varies as a function of z -position.
- Maximum instantaneous power consumption of 360 W .
- Detection is vulnerable to infrared noise.
- Inertial effects cause error accumulation.
- Controlled system exhibits overshoot and steady-state error.

The majority of the limitations are due to the mechanical aspect of the system and can be improved with further design and development.

Table 2: Experimentation results of system error accumulation.

Parameter	Axis		
	x	y	z
Waveform (m)	$0.1 \times \sin(2\pi(0.25)t)$		
Offset Error (mm)	0.938	3.73	2.5
Displacement (m)	6.8	6.8	6.8
Error (%)	0.0138	0.0549	0.0368
Waveform (m)	$0.1 \times \text{tri}(2\pi(0.375)t)$		
Offset Error (mm)	11.6	7.34	24.1
Displacement (m)	4.4	4.3	4.4
Error (%)	0.264	0.171	0.548

6 Conclusion

The objective of remote surgery is tested through the design and implementation of a relatively inexpensive robotic arm. The robotic arm consists of the detection system, which is implemented using the Nintendo Wii remote technology, and the actuation system which is implemented using a lead screw design. The robotic arm is able to track the surgeon's forearm with less than 1 mm steady-state error and with a rise time of less than 0.5 s . The non-linear static friction, however, creates a deadzone effect that delays the motion of the robotic arm by 0.35 s .

The detection and encoder resolutions are both submillimeter, which ensures that the robotic arm can move and operate precisely during surgery. The error accumulated in the system is below 4 mm when the robotic arm is operated smoothly and at slower speeds. The end-effector of the robotic arm could be further developed by including the surgeon's precise finger and hand movements measured using more sensors.

Acknowledgment

The authors would like to thank Professor David Rubin and Mr Harold Fellows at the University of Witwatersrand for their guidance, advice and support.

References

- [1] G. Bekey, R. Ambrose, V. Kumar, A. Sanderson, B. Wilcox, and Y. Zheng, “International assessment of research and development in robotics.” World Technology Evaluation Center, Inc, Tech. Rep., 2006.
- [2] D. Holt, A. Z. J. Abramson, and R. Somogyi, “Robotic surgery and tele-surgery: Basic principles and description of a novel concept.” *University of Toronto Medical Journal*, vol. 82, no. 1, pp. 52–54, December 2004.
- [3] A. Mulder, “Hand centered studies of human movement project human movement tracking technology.” Simon Fraser University, Tech. Rep., 1994.
- [4] Y. Tao and H. Hu, “3D arm motion tracking for home-based rehabilitation.” Proceedings of the 3rd Cambridge Workshop on universal access and assistive technology, Tech. Rep., April 2006.
- [5] J. Rosen, M. Lum, and D. Trimble., “Spherical mechanism analysis of a surgical robot for minimally invasive surgery analytical and experimental approaches.” University of Washington, Seattle, Tech. Rep., January 2005.
- [6] B. Challacombe and P. Dasgupta, “Telemedicine-the future of surgery.” *The Journal of Surgery*, vol. 1, no. 1, pp. 15–17, 2003.
- [7] A. Pantanowitz., “Surgery environment assistant and automated control using infrared light tracking.” University of Witwatersrand, Johannesburg, Tech. Rep., 2008.
- [8] K. W. Hollander and T. G. Sugar, “Design of lightweight lead screw actuators for wearable robotic applications.” *Journal of Mechanical Design by the Arizona State University*, vol. 128, no. 1, pp. 644–648, 2006.
- [9] P. C. Sen, *Principles of Electric Machines and Power Electronics.*, 2nd ed. John Wiley and Sons, 1997.

- [10] SLA7024M, Datasheet, “Two-Phase Stepper Motor Unipolar Driver IC,” <http://www.datasheetcatalog.com>, Last accessed 11 October 2009.
- [11] FLRS-770PM-7038, Datasheet, “DC brush motor.” <http://www.mantech.co.za>, Last accessed 26 September 2009.
- [12] JRS-550PM-7024, Datasheet, “Fulling DC brush motor.” <http://www.mantech.co.za>, Last accessed 26 September 2009.
- [13] R. S. Burns, *Advanced Control Engineering.*, 1st ed. Butterworth-Heinemann, 2001, ch. 4, p. 91.